Modeling the Response of Turbulent Flames to Harmonic Forcing

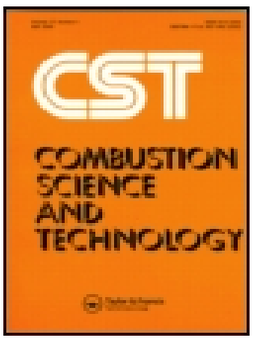

Taylor & Francis
Taylor & Francis Group

Combustion Science and Technology

ISSN: 0010-2202 (Print) 1563-521X (Online) Journal homepage: http://www.tandfonline.com/loi/gcst20

Modeling the Response of Turbulent Flames to Harmonic Forcing

Luke J. Humphrey, Vishal S. Acharya, Dong-Hyuk Shin & Timothy C. Lieuwen

To cite this article: Luke J. Humphrey, Vishal S. Acharya, Dong-Hyuk Shin & Timothy C. Lieuwen (2016): Modeling the Response of Turbulent Flames to Harmonic Forcing, Combustion Science and Technology, DOI: 10.1080/00102202.2016.1202245

To link to this article: http://dx.doi.org/10.1080/00102202.2016.1202245

Accepted author version posted online: 22 Jun 2016.
Published online: 22 Jun 2016.

Modeling the Response of Turbulent Flames to Harmonic Forcing

Luke J. Humphrey[a], Vishal S. Acharya[a], Dong-Hyuk Shin[b], Timothy C. Lieuwen[a]

[a]School of Aerospace Engineering
Georgia Institute of Technology
Atlanta, GA, USA 30318

[b]School of Engineering
University of Edinburgh
HOSAAO
Max Born Crescent
Edinburgh, EH9 3BF

Corresponding author: Timothy Lieuwen
Ben T. Zinn Aerospace Combustion Laboratory
School of Aerospace Engineering
Georgia Institute of Technology
635 Strong St NW, Atlanta, GA, USA 30318
Email: tim.lieuwen@aerospace.gatech.edu
Phone: 404-894-3041

Abstract

This paper analyzes the response of a turbulent, premixed flame to harmonic forcing. This problem has been worked extensively for laminar flames, and the key parameters influencing the flame transfer function are well understood. For turbulent flames, several prior studies have utilized a "quasi-laminar" approach, by utilizing the time-averaged flame position, and ensemble-averaged disturbance field, as inputs to what is otherwise identical to the laminar problem. More generally, the manner in which turbulent flames respond to harmonic disturbances is not amenable to analytical solutions because of the nonlinear interactions between stochastic flow disturbances and harmonic flame wrinkling. We utilize a turbulent burning velocity closure proposed by Shin and Lieuwen (2013), who showed that the ensemble-averaged turbulent burning rate for a harmonically forced flame is proportional to the ensemble-

averaged flame curvature. Shin and Lieuwen (2013) previously used it to analyze the ensemble-averaged space-time flame wrinkle characteristics. Here we extend these results to analyze the spatial variation of ensemble-averaged flame surface area and burning rate and then compare these results to computations. These results show that, for low stochastic forcing amplitudes, wrinkling of the front exerts quantitative differences between those predicted by a quasi-laminar and the actual flame response (e.g., reducing peak values of the flame transfer function, and eliminating nodes), but does not change the key qualitative features. While this result needs to be considered for strongly turbulent flames, it does suggest why good agreement has been observed between quasi-laminar approaches and experimental data for harmonically excited, turbulent flames. Two results for model problems showing the linearized flame transfer functions are also presented, which explicitly demonstrate qualitative turbulence effects on harmonically excited flames.

Keywords: Turbulent heat release, transfer function, level-set, quasi-laminar.

Nomenclature

ω_d	angular forcing frequency
$u_{x,n,s}$	axial, normal, and tangential velocity components, respectively.
ξ_1	coherent flame position fluctuation
u_C	convective velocity disturbance phase speed
a	coherent forcing amplitude
$u_{s,eff}$	effective tangential velocity
$\langle c \rangle$	ensemble-averaged flame curvature
$\hat{\varepsilon}_{ref}$	ensemble-averaged amplitude of flame holder, in flame normal direction
ε	excitation amplitude
l_0	excitation normalization length

s, n, z	flame axis, flame normal, and transverse coordinates
$s_{I,W}$	flame axis integration start location or end (wall) location
FDF	flame describing function
L_f	flame integration length
FTF	flame transfer function
G	flame transfer or describing function gain
$G_{I/W/S/Tot}$	flame transfer function gain components due to the starting correction (I), end (wall) correction (W), consumption speed (S), and the sum of the individual components (Tot)
$\vec{u}$	flow velocity
f_0	forcing frequency
$\hat{\xi}'$	Fourier space flame position fluctuation
$\Delta\hat{s}_{I,W}$	Fourier space integration limit start or end correction
Δh_R	heat of combustion per unit mass
$\underline{Q}'_{A,S}$	heat release fluctuation due to area (A), or flame speed (S)
ξ	instantaneous flame position
L_{11}	integral length scale
S_L	laminar local burning velocity
ξ_0	mean flame position
γ	non-dimensional convective velocity disturbance amplitude decay rate
$\hat{l}'_{ref}$	reference excitation length
$St_{I/W/L_f}$	$\left(\omega_d \cdot s_{I,W,L_f}\right)/u_{s,0}$ = Strouhal number based on s_I, s_W, or L_f
$S_{T,D/C}$	turbulent displacement (D) or consumption (C) speed
$\overline{C}$	turbulent flame progress variable
$\sigma_{T,D/C}$	turbulent Markstein displacement (D) speed length or consumption (C) speed length
ΔL_f	two-dimensional flame length fluctuation
ρ	unburned density
$S_{T,0/C0}$	uncurved turbulent flame displacement (0) or consumption speed ($C0$)
θ_0	unforced flame angle

I. Introduction

This paper describes an analysis of the ensemble-averaged flame position and heat release dynamics of harmonically forced, turbulent, premixed flames. Thermoacoustic oscillations are a key motivator for this work, as these self-excited oscillations involve the feedback of narrowband acoustic oscillations with vortices and the flame (Candel, 2002, Ducruix et al., 2003, Lieuwen and Yang, 2005). The least understood part of the internal feedback loop leading to these oscillations is how flames respond to these narrowband oscillations. A significant literature now exists on the response of laminar flames to harmonic flow disturbances, and the key physics controlling both the local space-time dynamics of the flame position (Petersen and Emmons, 1961, Boyer and Quinard, 1990, Preetham et al., 2008, Shanbhogue et al., 2009, Shin and Lieuwen, 2012, Cuquel et al., 2013) and spatially integrated heat release (Fleifil et al., 1996, Ducruix et al., 2000, Schuller et al., 2003, Kashinath et al., 2013) is well understood. However, real flames inevitably exist in a turbulent flow environment and so the flame is simultaneously disturbed by both spatio-temporally narrow and broadband disturbances. Because the flame dynamics are nonlinear, the influence of these disturbances on the flame cannot be treated additively.

In order to set up the problem, consider Fig. 1, which shows a flame spreading from a stabilization point. If the flame is weakly wrinkled, it is possible to define its instantaneous location by the single valued function ξ. In addition, we can define the spatially integrated heat release as Q^*. We can write each of these variables, ($\vec{u}, \xi, Q$), as the following triple decomposition, shown here for flow velocity:

*As noted in Humphrey et al. (2014), multiple definitions for the spatially integrated heat release exist, depending upon one's assumptions of the potentially oscillating integration limits. We will assume here that flames are confined and spread to the wall and so the transverse integration limits are fixed, implying that the axial integration limits oscillate.

$$\vec{u}(\vec{s},t) = \vec{u}_0(\vec{s}) + \vec{u}_1(\vec{s},t) + \vec{u}_2(\vec{s},t) \tag{1}$$

Where $(\ )_0$ is the time-averaged quantity, defined as:

$$\vec{u}_0(\vec{s}) = \frac{1}{T}\int_0^T \vec{u}(\vec{s},t)\,dt \tag{2}$$

The second quantity, $(\ )_1$, is the coherent fluctuation and is defined using the ensemble average, denoted by the operator $\langle\ \rangle$, as:

$$\vec{u}_1(\vec{s},t) = \langle \vec{u}(\vec{s},t) - \vec{u}_0(\vec{s}) \rangle \tag{3}$$

And, the random fluctuation, $(\ )_2$ is then:

$$\vec{u}_2(\vec{s},t) = \vec{u}(\vec{s},t) - \vec{u}_0(\vec{s}) - \vec{u}_1(\vec{s},t) \tag{4}$$

Note that $(\vec{u}_1)_0 = (\vec{u}_2)_0 = 0$, $\langle \vec{u}_2 \rangle = 0$, but $\langle \vec{u}_1 \rangle \neq 0$. Note also that for this harmonically forced problem, the "ensemble-average" is equivalent to a "phase-average".

The key problem of interest to this paper is the input-output relation between the coherent velocity forcing and the coherent fluctuations in flame position and heat release; e.g., for the spatially integrated heat release of a flame forced by flow disturbances:

$$FDF\ (a,\omega_d) = \frac{\langle \hat{Q}_1 \rangle / Q_0}{\langle \hat{u}_1 \rangle / u_0} \tag{5}$$

where the $\hat{\ }$ denotes the Fourier transformed variable, a is the amplitude of coherent excitation, and ω_d is the angular driving frequency. Equation (5) denotes the global flame describing function (*FDF*) of the turbulent, premixed flame. In the linear, small forcing amplitude limit, the *FDF* is amplitude independent and denoted as the global flame transfer function, *FTF*. This *FTF* and/or *FDF* is what is measured in the numerous data now available on the response of premixed flames to harmonic forcing (Fleifil et al., 1996, Ducruix et al., 2000,

Schuller et al., 2002, Lipatnikov and Sathiah, 2005, Kornilov et al., 2007, Preetham et al., 2010, Jones et al., 2011, Acharya et al., 2013, Acharya et al., 2014), such as shown in Fig. 2, for a swirl-stabilized flame.

This problem - i.e., the input-output relation between the coherent velocity forcing and the coherent fluctuations in flame position and heat release of turbulent flames- has been previously addressed both implicitly and explicitly. Hemchandra et al. (2007) was the first study we are aware of which explicitly considered the ensemble-averaged response of a flame forced by simultaneous broadband and narrowband disturbances. A related follow on study was also reported by Hemchandra et al. (2011). The first of these studies demonstrates that one of the key effects of the broadband disturbances, $\vec{u}_2$, on $\langle Q \rangle$ is through its influence on the time-averaged flame shape. This particular effect can be modeled by treating the flame as laminar and considering its response to harmonic forcing, but using the time-averaged turbulent flame properties as inputs to the flame shape – this is referred to as a "quasi-laminar" approach below[†]. In addition, flame wrinkles induced by the random fluctuations increase the destruction rate of the coherent wrinkles due to harmonic forcing, such as shown in Fig. 6. Thus, the effects of turbulence and harmonic forcing are not simply additive but are nonlinearly coupled. Shin and Lieuwen (2013) subsequently analyzed the explicit dynamic influences of turbulence on the ensemble-averaged flame dynamics and showed that, for flames with constant *local* laminar burning velocities, background broadband forcing leads to an effect on the ensemble-averaged flame position that is equivalent to a modulation in turbulent burning velocity, proportional to the local ensemble-averaged curvature. In other words:

[†] Note that an analogous approach is sometimes used in the hydrodynamic stability literature, where the time averaged velocity profile of a turbulent flow is used as an input to a stability calculation to determine the growth rate of a harmonic space/time disturbance; see discussion of this approach in, e.g., Refs. (Barkley, 2006, Meliga et al., 2012, Mettot et al., 2014)

$$S_{T,D}(s,t) = S_{T,0}(s)\left(1-\sigma_{T,D}(s)\langle c(s,t)\rangle\right), \tag{6}$$

where $S_{T,D}$ is the ensemble-averaged turbulent displacement speed (defined in Eq. (11)), and $\langle c \rangle$ is the ensemble-averaged flame curvature. Due to its analogy with the stretch sensitivity of laminar flames, $\sigma_{T,D}$ is denoted as the turbulent displacement Markstein length (although the local, instantaneous burning velocity is stretch independent in this calculation). Note that this modulation of the ensemble-averaged turbulent burning velocity is not captured by quasi-laminar approaches.

In addition, several experimental studies have used measured velocity fields as inputs to the level-set equation to predict flame position (Acharya et al., 2013) and *FDF's* (Acharya et al., 2014). These *FDF's* were also directly measured and compared to the predictions. These approaches used the measured ensemble-averaged velocity field as inputs to the level-set equation, and the mean turbulent flame position as parameters. As noted above, this quasi-laminar approach accounts for turbulent background effects on time-averaged flame properties and ensemble-averaged fluctuating quantities, but does not incorporate any dynamical effects. These analyses showed quite good agreement with the predictions and measurements, suggesting that the key impact of the turbulent background is on the time-averaged flame/flow properties.

The objective of this study is to analytically consider this problem further. The spatially integrated heat release, $\langle Q(t) \rangle$, of a turbulent, premixed flame, is examined by modeling the ensemble-averaged flame response, using Shin and Lieuwen's (2013) ensemble-averaged turbulent flame speed closure, Eq. (6), discussed above.

Both the numerical and analytical analysis here is restricted to isothermal flames. For real flames, heat release, and the resulting density change, alters the approach flow, and there is a

significant body of work which discusses this effect (Matalon and Matkowsky, 1982, Peters et al., 2000, Lee and Lieuwen, 2003, Creta et al., 2011).

Realistically, flames generally have non-zero heat release, density, and temperature jumps. However, it should be noted that the isothermal limit is interesting for its own sake, as there are practical applications such as vitiated flow or highly compressed flows with small temperature and density jumps. A non-zero density jump introduces an important effect, the Darrieus-Landau flame instability, resulting from changes in the approach flow which cause flame wrinkle amplification (Matalon and Matkowsky, 1982). In addition, heat release for a ducted flame causes acceleration of the flow, causing the velocity field to vary spatially along the flame.

As the focus of this paper is on the influence of the stochastic flame wrinkling induced by turbulent velocity fluctuations upon the coherent wrinkles induced by the harmonic flow disturbances, these assumptions enable us to focus on the flame dynamics problem, without the added complication of the modifications of the flow field induced by the moving flame.

The rest of this paper is organized as follows. First, a description of the ensemble-averaged flame position equation and its use in defining the ensemble-averaged turbulent flame speed are given. Next, the problem geometry, introduced above is elaborated on, followed by a description of the numerical procedure, and an explanation of the calculation of the global heat release. Validation of the proposed flame speed closure and modeling approach is provided by a direct comparison of flame shape and heat release between the numerical simulation and the analytical model in Sec. IV. The use of the flame speed closure is further examined with two model problems in section V: (1) the development of a linear model from the general analytical model presented in Sec. IV and (2) application of these results to a flame perturbed by a convecting, decaying vortex. A discussion of the results is also given in Sec. V.

II. Ensemble-averaged Flame Position Equation

The front-tracking equation is the key analytical tool used to analyze the flamelet dynamics in this study. This approach is commonly used in other studies of flame kinematics (Boyer and Quinard, 1990, Fleifil et al., 1996) and is well-developed (Matalon and Matkowsky, 1982, Williams, 1985, Kerstein et al., 1988, Peters et al., 2000, Lipatnikov and Sathiah, 2005). For high activation energy molecular kinetics, the flame becomes thin relative to the scales of the flow and can be treated as a flow discontinuity. In this approach, the flame is defined as the zero surface given by the *G*-equation:

$$\frac{\partial G}{\partial t} + \vec{\boldsymbol{u}} \cdot \vec{\nabla} G = S_L \left| \vec{\nabla} G \right| \tag{7}$$

where $\vec{\boldsymbol{u}}$ is the flow velocity at the flame front, and S_L denotes the local propagation front speed. For a single valued flame position (note that our computational results shown later do not assume a single valued flame position), this equation can be written as:

$$\frac{\partial \xi}{\partial t} + u_s \frac{\partial \xi}{\partial s} - u_n + u_z \frac{\partial \xi}{\partial z} = S_L \left[1 + \left(\frac{\partial \xi}{\partial z} \right)^2 + \left(\frac{\partial \xi}{\partial s} \right)^2 \right]^{1/2} \tag{8}$$

Ensemble averaging this equation leads to:

$$\frac{\partial \langle \xi \rangle}{\partial t} + \left\langle u_s \frac{\partial \xi}{\partial s} \right\rangle - \langle u_n \rangle + \left\langle u_z \frac{\partial \xi}{\partial z} \right\rangle = \left\langle S_L \left[1 + \left(\frac{\partial \xi}{\partial z} \right)^2 + \left(\frac{\partial \xi}{\partial s} \right)^2 \right]^{1/2} \right\rangle \tag{9}$$

Note that analyzing the ensemble-averaged flame position, $\langle \xi \rangle$, as shown in Eq. (9), leads to the same "closure" problem as found in most nonlinear problems, such as in the Reynolds-Averaged Navier-Stokes (RANS) equations. As such, Shin and Lieuwen (2013) computationally solved the *G*-equation, Eq. (7) (i.e., they did not assume that the flame was instantaneously single valued) for a flame with constant laminar burning velocity, S_L, and post-processed the ensemble-

averaged results. In analogy with Eq. (8), above, they wrote the following equation relating ensemble-averaged flame position to the ensemble-averaged disturbance field:

$$\frac{\partial\langle\xi\rangle}{\partial t}+\langle u_s\rangle\frac{\partial\langle\xi\rangle}{\partial s}-\langle u_n\rangle+\langle u_z\rangle\frac{\partial\langle\xi\rangle}{\partial z}=s_{T,D}(s,z,t)\left[1+\left(\frac{\partial\langle\xi\rangle}{\partial z}\right)^2+\left(\frac{\partial\langle\xi\rangle}{\partial s}\right)^2\right]^{1/2} \tag{10}$$

There are no assumptions in this equation; rather it *defines* the turbulent displacement speed, $s_{T,D}$, which can be seen by rearranging the above as:

$$s_{T,D}(s,z,t)\equiv\frac{\frac{\partial\langle\xi\rangle}{\partial t}+\langle u_s\rangle\frac{\partial\langle\xi\rangle}{\partial s}-\langle u_n\rangle+\langle u_z\rangle\frac{\partial\langle\xi\rangle}{\partial z}}{\left[1+\left(\partial\langle\xi\rangle/\partial z\right)^2+\left(\partial\langle\xi\rangle/\partial s\right)^2\right]^{1/2}} \tag{11}$$

where $\langle\xi\rangle$ is the ensemble-averaged flame position, and *s* is the downstream coordinate for a coordinate system aligned with the unforced flame position, and *z* is the transverse coordinate, parallel with the flame holder, as shown in Fig. 1. The use of Eqs. (10) and (11) requires the ensemble-averaged flame to remain single-valued, which introduces an upper limit on harmonic forcing amplitude, but does not require the instantaneous flame to remain single-valued, as shown in Fig. 3. Empirical post-processing of their computational results led to the model equation for $s_{T,D}$ shown in Eq. (6). Some of these results are reproduced in Fig. 5 and discussed further in Sec. III.D.

Having considered the flame position, we next consider its heat release. The ensemble-averaged, spatially integrated heat release is given by the expression:

$$Q(t)=\left\langle\int_{s_I(t)}^{s_W(t)}\rho\Delta h_r S_L\,dA\right\rangle \tag{12}$$

where ρ is the unburned gas density, Δh_R is the heat of combustion per unit mass, and *dA* is the area element. The integration limits, $s_I(t)$ and $s_W(t)$ are time dependent, reflecting the potential

motion of both the flame stabilization point and flame length. Assuming constant density and heat of reaction, we *define* the turbulent consumption speed, $S_{T,C}$ through the following relation:

$$\int_{\langle s_I(t)\rangle}^{\langle s_W(t)\rangle} S_{T,C}(t,s)\langle dA\rangle \equiv \left\langle \int_{s_I(t)}^{s_W(t)} S_L dA \right\rangle \tag{13}$$

Although $S_{T,C}$ was not analyzed by Shin and Lieuwen (2013), results presented in Sec. III.D show that it exhibits a similar sensitivity to ensemble-averaged flame curvature, $\langle c\rangle$, although the proportionality constant is not exactly equal to $\sigma_{T,D}$.

III. Numerical Calculations – Oscillating Flame Holder

A. Geometry

Following Shin and Lieuwen (2013), we consider first the problem of an oscillating flame holder (Petersen and Emmons, 1961, Kornilov et al., 2007, Kanthasamy et al., 2012). This is an important canonical problem for understanding flame response physics, because the oscillating flame holder is the only flame wrinkle excitation source, and leads to a traveling wave that convects down the flame. The magnitude of this flame wrinkling traveling wave is constant when considering a constant density, constant burning velocity, linear analysis. A number of studies have investigated *FDFs* where forcing is induced by velocity fluctuations (Preetham et al., 2008, Wang et al., 2009). In this case, the flame is excited simultaneously over its entire length and the resulting flame wrinkle amplitude exhibits spatial interference patterns. These interference patterns complicate the analysis of flame wrinkle destruction behavior, as multiple processes can lead to reduction in flame wrinkling amplitude. Thus, the simplification afforded by use of flame anchor excitation facilitates identification of key problem variables. We will consider the more physically interesting velocity forced flame problem in Sec. V.B.

Consider the geometry shown in Fig. 1, where a flame is attached to a harmonically oscillating bluff-body, and spreads to the wall. Figure 3 shows two snapshots of the instantaneous, multi-valued flame, and the corresponding ensemble-averaged result at that same phase of the harmonic forcing cycle. Note that at high turbulence intensities, the instantaneous flame may become highly multi-valued and is three-dimensional. In this case, the ensemble-averaged result remains single-valued (but not necessarily in general) and is two-dimensional.

As discussed in the earlier footnote*, the area integration is taken over a fixed width (rather than fixed length, or fixed axial distance), which is the most physically relevant problem for confined combustion problems. The inclusion of end correction factors accounts for flame area fluctuations which occur as a wrinkled flame intersects a wall.

The unforced burning area is based on the two-dimensional area of the flame, equal to the flame length. It is calculated as the time-averaged length of the mean flame, integrated between the oscillating end points:

$$L_f = \left[\int_{s_I(t)}^{s_W(t)} \left(\left(\frac{\partial \xi_0}{\partial s} \right)^2 + 1 \right)^{1/2} ds \right]_0 \tag{14}$$

This flame length is used to calculate the Strouhal number, $St_{Lf} = \left(L_f \cdot \omega_d \right) / u_{s,0}$.

B. Numerical Procedure

This section describes the numerical approach used to compute the space-time dynamics of the flame position and heat release. Analysis of the ensemble-averaged space-time dynamics of the flame position, $\langle \xi \rangle$, was previously presented by Shin and Lieuwen (2013); here we consider also the heat release. The key assumptions for this analysis are that (1) S_L is constant (2) the flame remains attached to the harmonically oscillating flame holder (3) isothermal flow field, as discussed in Sec. I .

As described by Shin and Lieuwen (2013), the level-set equation is solved with a semi-Lagrangian Courant-Isaacson-Rees (CIR) scheme, using the back-and-forth error correction and compensation (BFECC) method (Dupont and Liu, 2007). The computational domain size is 201 x 201 x 801, and the time step is 1/(1000 f_0), where f_0 is the forcing frequency. The spatial resolution is greater than $\left(u_{s,0}/f_0\right)/100$, $L_{11}/10$. Grid convergence was determined for several cases; for a laminar baseline case, less than 1% difference in flame position was obtained with a factor-of-ten increase in grid density at $s/\left(u_{s,0}/\omega_d\right)=25$. A second case was conducted with a turbulence intensity of $u_{RMS}/u_{s,0}=0.04$, and a factor-of-two increase in grid density, showed a 3% difference in the ensemble-averaged flame position at $s/\left(u_{s,0}/\omega_d\right)=15$.

As discussed in Shin and Lieuwen (2013), different approaches have been used in the past to determine ensemble-averaged flame positions. One approach is to binarize the *G*-fields between products and reactants and then average these fields. The averaged field is then associated with a progress variable (e.g. $\overline{C}$), and the ensemble-averaged flame position defined at some progress variable value, such as $\overline{C}=0.5$. However, this approach results in a progress variable which defines a median rather than mean value of the flame position. As this creates some complications when comparing with analytical results, we extract the instantaneous flame position coordinates and define the flame position as the average transverse value at each axial location. The ensemble-averaged flame position results from ensemble averaging over 160 forcing cycles.

For the oscillating flame holder problem, the flow field consists of the superposition of a spatially uniform field with a stochastic component, but with no coherent component; i.e.

$$\vec{\boldsymbol{u}}\left(\vec{\boldsymbol{s}},t\right)=\vec{\boldsymbol{u}}_0\left(\vec{\boldsymbol{s}}\right)+\vec{\boldsymbol{u}}_2\left(\vec{\boldsymbol{s}},t\right) \tag{15}$$

The stochastic velocity fluctuations are isotropic, incompressible, and Gaussian distributed with spatial correlation lengths that decay exponentially over a longitudinal, integral length scale; i.e.

$$\frac{\left\langle u_{x,2}\left(x,n,z,t\right)u_{x,2}\left(x+r,n,z,t\right)\right\rangle}{\left\langle u_{x,2}{}^{2}\right\rangle}=\exp\left(-\frac{\pi}{4}\left(\frac{r}{L_{11}}\right)^{2}\right) \tag{16}$$

The flow convects these disturbances with the mean flow velocity as-per Taylor's hypothesis, and so the integral time and length scales are directly related through the mean flow velocity. As such, while these disturbances are stochastic, the fact that they are single length/time scale implies that they do not describe Navier-Stokes turbulence. However, this general structure of the correlation function is used routinely in the turbulence literature, e.g., see (Hinze, 1975) and (Pope, 2000). These flow disturbances are used as inputs to solve Eq. (7) – note that the fact that the flow field is imposed upon the flame, as opposed to being simultaneously solved with the flame implies negligible gas expansion across the flame, as discussed above. Additional discussion of the numerical method and turbulence field are given in Shin and Lieuwen (2013). The outputs of these calculations are instantaneous flame positions and areas.

C. Numerical Heat Release Calculations

Because the numerical calculations all assume constant local burning velocity, S_L, and mixture composition, heat release is directly proportional to instantaneous flame surface area. To calculate the numerical flame area, the instantaneous flame position and area (with area data extracted from the multi-valued numerical simulation) are averaged in the transverse direction. Because the discretization of the flame position and area along the *s*-coordinate does not generally align with a desired integration point on the *y*-axis, the flame position is interpolated between adjacent *s*-locations where it crosses the integration limits. The area fluctuation is

determined by taking the Fourier transform of the entire area time signal. This area is then normalized by L_f, the two-dimensional unforced area, which again is proportional to the burning rate.

The maximum area fluctuation occurs when out of phase wrinkle anti-nodes exist at the integration limits, at a given instant in time, as illustrated in Fig. 4. This maximum flame length fluctuation, normalized by the flame length, L_f is:

$$\frac{\Delta L_f}{L_f} = \frac{2\varepsilon}{L_f \cdot \tan(\theta_0)} \tag{17}$$

Equation (17) is equal to the denominator of the *FDF*, which is defined as:

$$G = \frac{\hat{Q}_1 / Q_0}{\hat{\varepsilon}_{ref} / l_0} \tag{18}$$

where ε_{ref} denotes the amplitude of displacement of the flame holder in the flame normal direction. Note that setting Eq. (17) equal to the denominator in Eq. (18), and solving for l_0, provides the appropriate reference length scale.

$$l_0 = \frac{L_f \tan(\theta_0)}{2} \tag{19}$$

D. Numerical Calculation of Turbulent Parameters

As discussed above in the context of Eq. (6), in the far-field, $S_{T,D}$ shows curvature dependence analogous to that of stretch sensitive laminar flames with positive Markstein lengths (Shin and Lieuwen, 2013). This section briefly shows several illustrative calculations demonstrating this dependency.

Figure 5 shows illustrative calculations, plotting the joint probability density functions of the turbulent flame speed and ensemble-averaged curvature, $\langle c \rangle$. Results are shown for both $S_{T,D}$ and $S_{T,C}$ for the locations $s/(u_{s,0}/\omega_d) \cong 10.2 - 35.3$ at which $S_{T,D}$ and $S_{T,C}$ approach a constant value (near

the flame holder, both the burning velocities and turbulent Markstein lengths change substantially). This result demonstrates the clear correlation between the instantaneous flame speed and ensemble-averaged curvature. The line is a least-squares best fit through the simulation results. The simulations show that $S_{T,D}$ and $S_{T,C}$ (and therefore $\sigma_{T,D}$ and $\sigma_{T,C}$) have similar dependencies on turbulence intensity and instantaneous curvature, with $S_{T,C}$ greater than or equal to $S_{T,D}$ by about 10-45%, depending on turbulent intensity. Note that the figure uses data from multiple spatial locations, while the parameters used for the calculations described in Sec. IV are calculated locally, at each spatial location. These results show that the consumption speed, like the displacement speed, demonstrates an approximately linear sensitivity to ensemble-averaged curvature and can be modeled as:

$$S_{T,C}(s,t) = S_{T,C0}(s)\left(1-\sigma_{T,C}(s)\langle c(s,t)\rangle\right) \tag{20}$$

where $\sigma_{T,C}$ is the turbulent consumption speed length, and $S_{T,C0}$ is the uncurved consumption speed.

From these results, the value of $S_{T,0}$ in Eq. (6) is determined by extrapolating $S_{T,D}$ to zero curvature. At each spatial location, the turbulent displacement Markstein length, $\sigma_{T,D}$ and turbulent consumption Markstein length $\sigma_{T,C}$ are calculated by determining the slope of the regression between $S_{T,D}$ (or $S_{T,C}$) and the ensemble-averaged curvature, $\langle c\rangle$, and then dividing by the value of $S_{T,0}$ or $S_{T,C0}$, for the displacement or consumption Markstein length, respectively. These extracted local values of $S_{T,0}$, $S_{T,C0}$, $\sigma_{T,D}$ and $\sigma_{T,C}$ are used in the reduced order model discussions in the next sections. Additional results and discussion of these trends, as well as a physical explanation of why this correlation occurs, is described in our earlier publication (Shin and Lieuwen, 2013) and so we do not go into further details here.

IV. Analytical Model Development and Validation

This section describes the development of a reduced order model for $\langle Q \rangle$, utilizing the turbulent flame speed models described above. The results of this model are compared to computed results for flame position and $\langle Q \rangle$ in Sec. IV.B and IV.C, respectively.

A. Formulation

We can use the equations for the ensemble-averaged flame position, Eq. (10), and heat release Eqs. (12) and (13) along with the closures for the turbulent displacement and consumption speeds to solve for the *FDF*. In other words, the flame position is solved from the following expression, derived from Eqs. (6) and (10):

$$\frac{\partial \langle \xi \rangle}{\partial t} + \langle u_{s,eff} \rangle \frac{\partial \langle \xi \rangle}{\partial s} - \langle u_n \rangle + \langle u_z \rangle \frac{\partial \langle \xi \rangle}{\partial z} = S_{T,0}(s) \left(1 + \sigma_{T,D}(s) \frac{\partial^2 \langle \xi \rangle / \partial s^2}{\left[1 + \left(\partial \langle \xi \rangle / \partial s \right)^2 \right]^{3/2}} \right) \left[1 + \left(\frac{\partial \langle \xi \rangle}{\partial z} \right)^2 + \left(\frac{\partial \langle \xi \rangle}{\partial s} \right)^2 \right]^{1/2} \quad (21)$$

where $u_{s,eff}$ indicates the effective tangential velocity of the wrinkle (i.e. $u_{s,eff}$ is the slope of the phase of the ensemble-averaged flame wrinkle), which accounts for correlations between turbulent and harmonic fluctuations. This effect was not accounted for in the original publication of Shin and Lieuwen (2013) the correction is quite small but its effect compounds with distance from the flame holder. Also, note the definition of ensemble-averaged curvature, $\langle c \rangle$, so that flames oriented convex to the reactants have positive curvature, as typically defined for flamelets :

$$\langle c \rangle = -\frac{\partial^2 \langle \xi(s,t) \rangle / \partial s^2}{\left[1+\left(\partial \langle \xi(s,t) \rangle / \partial s\right)^2\right]^{3/2}} \tag{22}$$

This equation can be solved for a given disturbance field, and axial distribution of $S_{T,0}$ and $\sigma_{T,D}$. Having solved for $\langle \xi(s,t) \rangle$, the heat release can then be solved from the expression

$$Q(t) = \int_{\langle s_I(t) \rangle}^{\langle s_W(t) \rangle} \rho \Delta h_r S_{T,C0}(s) \left(1+\sigma_{T,C}(s)\frac{\partial^2 \langle \xi \rangle / \partial s^2}{\left[1+\left(\partial \langle \xi \rangle / \partial s\right)^2\right]^{3/2}}\right)\left(\left(\frac{\partial \langle \xi \rangle}{\partial s}\right)^2+1\right)^{1/2} ds \tag{23}$$

where we assume constant ρ and Δh_R. The *FDF* result then follows from inserting the computed heat release into Eq.(18). In order to evaluate the validity of the flame speed closures for the turbulent displacement and consumption speeds, the flame position and heat release response were compared to the numerical results, as shown in the following two subsections.

B. Model Evaluation: Flame Position

The turbulent flame speed closure was evaluated by integrating Eq. (21) for a two-dimensional geometry.

$$\frac{\partial \langle \xi \rangle}{\partial t} + \langle u_{s,eff} \rangle \frac{\partial \langle \xi \rangle}{\partial s} - \langle u_n \rangle = S_{T,0}(s)\left(1+\sigma_{T,D}(s)\frac{\partial^2 \langle \xi \rangle / \partial s^2}{\left[1+\left(\partial \langle \xi \rangle / \partial s\right)^2\right]^{3/2}}\right)\left[1+\left(\frac{\partial \langle \xi \rangle}{\partial s}\right)^2\right]^{1/2} \tag{24}$$

This equation was solved using a total variation diminishing (TVD) Runge-Kutta scheme, employing weighted, essentially non-oscillatory (WENO) derivatives and local Lax-Friedrichs flux (Jiang and Peng, 2000). Values of $S_{T,D}$ and $S_{T,0}$ at each spatial location, *s*, were extracted from the computed results, as described at the end of Sec. III.D. Similarly, the effective tangential velocity is calculated by extracting the wrinkle phase speed from the phase of the ensemble-averaged result.

Figure 6 shows a comparison between the flame fluctuation determined from ensemble-averaging of the numerical solution to the *G*-equation (solid line; discussed in Sec. III) and the predicted flame fluctuation determined from the analytical model (i.e. from integration of Eq. (24), dotted line), as well as the quasi-laminar result (dashed line).

The figure shows that the ensemble-averaged flame shape predicted from the analytical model agrees very well with the ensemble-averaged results directly extracted from the computations. For the two lower turbulence cases, the predicted flame shape is virtually identical. For the two higher turbulence intensity cases, there is some difference between the analytical and numerical predictions, the difference increasing with the flame coordinate, *s*.

In addition, Fig. 6 shows the results from a quasi-laminar analysis, which incorporates the spatial variation in $S_{T,0}$ but has no dynamical flame speed closure model (equivalent to setting $\sigma_{T,D} = 0$). The turbulent flame speed closure clearly improves the accuracy of the predicted flame position, even for the lowest turbulence intensity. These comparisons, therefore, demonstrate the validity of the turbulent Markstein length displacement speed closure, Eq. (6), discussed previously, for low to moderate turbulence intensities.

C. Model Evaluation: Heat Release

Further validation of the turbulent displacement speed closure, as well as of the turbulent consumption speed closure, which is closely related to heat release, is given by comparing the heat release characteristics of the numerical solution of the *G*-equation to those predicted by the analytical model. The numerical heat release is determined by integrating the instantaneous flame surface area over the integration domain, and finding the response at the forcing frequency using the Fourier transform of the area time signal. The flame area integration of the non-linear

analytical model is accomplished using a trapezoidal integration method. The values of $\sigma_{T,D}$, $\sigma_{T,C}$, $S_{T,0}$, and $S_{T,C0}$ used in the analytical model correspond to those calculated from numerical data simulated with the specified values L_{11}, u_{RMS} and harmonic forcing amplitude. The response at the forcing frequency is determined using the Fourier transform of the burning-rate weighted area time signal.

Figure 7 shows the gain and phase of the numerical (solid lines), analytical (dotted lines), and quasi-laminar (dashed lines) *FDFs*. Before discussing these results, it is important to explain how the laminar, constant flame speed flame holder forced response differs from the velocity forced one. The velocity forced *FTF* asymptotes to a value of unity as frequency tends to zero. This result can be understood from quasi-steady considerations – an increase in flow velocity of a fixed composition mixture causes a proportional increase in heat release rate. In contrast, the *FTF* of the flame holder forced flame asymptotes to zero as frequency tends toward zero, since the quasi-steady heat release is invariant to flame holder position. Similarly, the gain of the velocity forced *FTF*, while exhibiting some interference patterns, has a general low pass filter character, decaying as *1/St*. This occurs because the magnitude of particle displacement, and consequent flame wrinkling scales as u'/f, and so doubling the frequency at a fixed velocity disturbance magnitude halves the magnitude of displacement fluctuations. In contrast, the *displacement* is forced for the oscillating flame holder problem, and so the magnitude of flame wrinkling does not roll off with frequency when normalized by displacement amplitude. Similar to the velocity forced case, the gain of the laminar *FTF* is modulated due to phase cancellation effects associated with integration.

The analytical model correctly predicts the shape of the numerical *FDF*. Both the numerical solution and analytical model clearly indicate the role of phase cancellation effects in controlling

the gain, and the gain maxima and minima are well-aligned in Strouhal space. In addition, Fig. 7 shows that the model predicts two key qualitative effects of stochastic fluctuations: (1) a progressively decreasing maximum, and increasing minimum, of the *FDF* with increasing Strouhal number, and (2) a slight shift in the position of the node and anti-node locations in Strouhal space, associated with higher turbulence intensity. These effects are also present in the simulations, and are discussed further in the context of the linearized model problem presented in Sec. V.A

The phase results also are quite similar between the model and the computations - namely, the linearly increasing phase with frequency, the jump in phase across the gain minima, and the smoothing effect of the stochastic fluctuations on this phase jump.

In addition to the analytical and numerical results, Fig. 7 shows the results from the quasi-laminar approach, which are nearly identical to those of the analytical model, for $u_{RMS}/u_{s,0} = 0.021$. However, the model shows a significant improvement in prediction of gain maxima over those of the quasi-laminar approach with respect to the numerical results, at $u_{RMS}/u_{s,0} = 0.082$. Nonetheless, this close concurrence between the quasi-laminar result and the analytical model result suggests why quasi-laminar approaches have been so successful in comparisons of experimental data and models. Apparently, the "averaging" inherent in calculation of a global quantity, such as heat release, minimizes the importance of this turbulent flame speed modulation induced by turbulent fluctuations.

V. Results: Model Problems

The purpose of the prior section was to evaluate the closures presented in Eq. (6) and (20) in terms of predicting the phase-averaged flame position and heat release response obtained from

phase averaging the full computations. The purpose of this section is to analyze two model problems and to obtain analytical solutions that explicitly illustrate turbulence impacts on the *FTF*. Such explicit solutions are not possible in general, such as for the comparison shown in the prior section, because the equations to be solved are nonlinear and have non-constant coefficients. This section considers the linearized problem with constant coefficients in order to obtain explicit solutions that show the form of the solution. The first problem is the linear analysis of the oscillating flame holder problem, addressed in the previous section. The second problem is the case of a velocity forced flame with a convecting, decaying velocity disturbance, and a stationary attachment point, a problem previously investigated for laminar flames (Shin et al., 2008, Wang et al., 2009, Preetham et al., 2010).

A. Model Problem: Flame Perturbed by an Oscillating Flame Holder

While the preceding general analysis (Sec. IV) required the use of numerical solutions to determine the spatio-temporal flame and heat release characteristics, here we simplify the above expressions in order to obtain explicit analytical results. The key additional assumptions for this model problem are that (4) $S_{T,0}$, $\sigma_{T,D}$, and $S_{T,C}$ are spatially constant, and (5) small amplitude disturbances so that results can be linearized. As in the prior section, for this oscillating flame holder problem, ensemble-average properties are two-dimensional and $\vec{u}_1 = 0$. Applying the additional assumptions (4) and (5) to Eq. (21), leads to:

$$\frac{\partial \langle \xi_1 \rangle}{\partial t} + u_{s,eff} \frac{\partial \langle \xi_1 \rangle}{\partial s} = S_{T,0} \sigma_{T,D} \frac{\partial^2 \langle \xi_1 \rangle}{\partial s^2} \tag{25}$$

Here, the $\langle\ \rangle$ are shown to again emphasize that this is the ensemble-averaged problem, but are not included for the following development. The problem is transformed to Fourier space using a definition for the fluctuating quantities as:

$$\xi_1(s,t) = \text{Real}\left\{\hat{\xi}_1'(s)\,\varepsilon e^{-i\omega_d t}\right\}. \tag{26}$$

where $\hat{\xi}_1'$ is the fluctuating Fourier-space ensemble-averaged flame position, and ε is a non-dimensional excitation amplitude. This equation is solved subject to the boundary condition:

$$\xi_1\left(s=0,t\right) = \text{Real}\left\{\varepsilon e^{-i\omega_d t}\right\}, \tag{27}$$

which stipulates that the flame remains attached to the moving flame holder at s = 0. The second boundary condition is that no disturbances flow from the end of the flame upstream – it will be described further below. The general solution is given by:

$$\hat{\xi}_1'(s) = Ae^{sR_1} + Be^{sR_2} \tag{28}$$

where

$$R_1, R_2 = \frac{u_{s,eff} \mp \left(u_{s,eff}{}^2 - 4i\omega_d S_{T,0}\sigma_{T,D}\right)^{1/2}}{2S_{T,0}\sigma_{T,D}} \tag{29}$$

Here, $u_{s,eff}$ is the flow velocity tangential to the unforced flame. The R_1 term corresponds to the solution with a wave moving downstream, while the term R_2 is associated with the wave moving upstream. This latter term is nonphysical and so the coefficient B that multiplies terms containing R_2 is set to zero. In the small $\sigma_{T,D}$ limit, the R_1 term can be expanded as:

$$R_1 = \frac{i\cdot\omega_d}{u_{s,eff}} - \frac{\sigma_{T,D}S_{T,0}\omega_d{}^2}{u_{s,eff}{}^3} + O(\sigma_{T,D})^2 \tag{30}$$

Hence the solution is as follows:

$$\hat{\xi}_1(s) = \varepsilon \exp\left[s\left(\frac{i\cdot\omega_d}{u_{s,eff}} - \frac{\sigma_{T,D}S_{T,0}\omega_d{}^2}{u_{s,eff}{}^3}\right)\right] \tag{31}$$

Thus, the solution for ξ_1 shows that a wrinkle present on the flame front convects in the s-direction at a velocity of $u_{s,eff}$ and decays exponentially at a rate proportional to $\sigma_{T,D}$.

Consider the heat release next which, when linearized, is given by:

$$Q(t) = \int_{s_{I,1}(t)}^{s_{W,1}(t)} \rho \Delta h_r S_{T,C0}(s) \left(1 + \sigma_{T,C}(s) \frac{\partial^2 \xi_1}{\partial s^2} \right) ds \tag{32}$$

The limits of integration oscillate due to wrinkles on the flame, and it is therefore necessary to introduce start and end corrections to the limits of integration, as discussed by Humphrey et al. (2014). The start and end corrections equal:

$$\Delta \hat{s}_{I,1} = -\frac{\varepsilon}{\tan(\theta_0)} e^{s_I R_1} \tag{33}$$

$$\Delta \hat{s}_{W,1} = -\frac{\varepsilon}{\tan(\theta_0)} e^{s_W R_1} \tag{34}$$

Assuming spatially constant $S_{T,C0}$ and $\sigma_{T,C}$, integration of Eq. (32) yields:

$$\hat{Q}_1(\omega_d) = \rho \Delta h_r S_{T,C0} \left(\underbrace{\Delta \hat{s}_{W,1}(\omega_d) - \Delta \hat{s}_{I,1}(\omega_d)}_{\hat{Q}_{A,1}} + \underbrace{\sigma_{T,C} \frac{\partial \hat{\xi}_1}{\partial s}\Big|_{\hat{s}_{I,1}(\omega_d)}^{\hat{s}_{W,1}(\omega_d)}}_{\hat{Q}_{S,1}} \right) \tag{35}$$

where we have decomposed the contributions of flame area and turbulent burning velocity fluctuations to the ensemble-averaged heat release. Normalizing these terms by the mean flame heat release, and ε / l_0 (see Eq. (18)), leads to the following flame area and turbulent burning velocity transfer functions:

$$\hat{G}_A(\omega_d) = \frac{1}{2}\left(e^{s_I R_1} - e^{s_W R_1}\right) = \frac{1}{2} e^{s_I R_1}\left(1 - e^{L_f R_1}\right) \tag{36}$$

$$\hat{G}_S(\omega_d) = \frac{1}{2}\tan(\theta_0)\sigma_{T,C} R_1 \left(e^{s_W R_1} - e^{s_I R_1}\right) = -\frac{1}{2} e^{s_I R_1}\left(1 - e^{L_f R_1}\right)\tan(\theta_0)\sigma_{T,C} R_1 \tag{37}$$

The total analytical linear transfer function is simply the sum of these two components.

$$\hat{G}_{Tot}(\omega_d) = \frac{1}{2} e^{s_I R_1}\left(1 - e^{L_f R_1}\right)\left(1 - \tan(\theta_0)\sigma_{T,C} R_1\right) \tag{38}$$

Using the small σ expansion derived in Eq. (30), this expression becomes:

$$\hat{G}_{Tot}\left(\omega_d\right)=\frac{1}{2}\exp\left[s_I\left(\frac{i\omega_d}{u_{s,eff}}-\sigma_{T,D}\frac{S_{T,0}\omega_d{}^2}{u_{s,eff}{}^3}\right)\right]\left(1-\exp\left[L_f\left(\frac{i\omega_d}{u_{s,eff}}-\sigma_{T,D}\frac{S_{T,0}\omega_d{}^2}{u_{s,eff}{}^3}\right)\right]\right)\left(1-\tan\left(\theta_0\right)\frac{i\omega_d\sigma_{T,C}}{u_{s,eff}}\right) \quad (39)$$

This equation is then non-dimensionalized according to the following scheme.

$$\begin{aligned}\tilde{s}&=s/\left(u_{s,eff}/\omega_d\right)\\ \tilde{\sigma}_T&=\sigma_T/\left(u_{s,eff}/\omega_d\right)\\ \tilde{S}_{T,D}&=S_{T,D}/u_{s,eff}\\ \tilde{c}&=c\cdot\left(u_{s,eff}/\omega_d\right)\end{aligned} \quad (40)$$

where all lengths are non-dimensionalized by $\left(u_{s,eff}/\omega_d\right)$, and all velocities by $u_{s,eff}$. Non-dimensional spatial lengths along the *s*-axis are denoted as Strouhal numbers, as described previously. The transfer function is then given by:

$$\hat{G}_{Tot}\left(\omega_d\right)=\frac{1}{2}e^{St_I\left(i-\tilde{S}_{T,0}\tilde{\sigma}_{T,D}\right)}\left(1-e^{St_{Lf}\left(i-\tilde{S}_{T,0}\tilde{\sigma}_{T,D}\right)}\right)\left(1-i\tan\left(\theta_0\right)\tilde{\sigma}_{T,C}\right) \quad (41)$$

Equation (38) and (41) are key products of this study – they show the explicit dynamical influence of stochastic background fluctuations on the ensemble-averaged heat release oscillations.

Figure 8 plots the magnitude and phase of G_{Tot} from Eq. (38). Also, $S_{T,C0}$ is assumed equal to $S_{T,0}$ for these calculations. Note that Figure 8, which illustrates the linearized flame response, cannot be directly compared to Fig. 7, which also includes nonlinear effects (leading to harmonics in the flame wrinkling spectrum and kinematic restoration) and is included to demonstrate the validity of the flame speed closure. The key dynamical effect of stochastic background disturbances enters through the turbulent Markstein length terms. Their influence on the model problem gain results can be seen most easily by working from the expansion in Eq. (39). The magnitude of the small σ expansion is:

$$\left|\hat{G}_{Tot}\left(\omega_d\right)\right| = \frac{1}{2} e^{-St_I \tilde{S}_{T,0} \tilde{\sigma}_{T,D}} \left(1 - \cos\left(St_{Lf}\right) e^{-St_{Lf} \tilde{S}_{T,0} \tilde{\sigma}_{T,D}}\right) \tag{42}$$

This expression shows two influences of $\sigma_{T,D}$. First, it causes a general decay in the gain through the term $e^{-St_I \tilde{S}_{T,0} \tilde{\sigma}_{T,D}}$. This decay in gain values at a fixed Strouhal number with increasing turbulence intensity is clearly evident in Fig. 8‡.

The second effect of stochastic fluctuations is to reduce the influence of the interference term, $1 - \cos\left(St_{Lf}\right) e^{-St_{Lf} \tilde{S}_{T,0} \tilde{\sigma}_{T,D}}$; thus, increasing $\sigma_{T,D}$ causes the turbulent flame *FTF* to reduce its peak values, but also to increase the gain minima. Again, both of these effects are evident in Fig. 8. For example, the calculation results in the figure show that the first maximum drops from a value of 1 to about 0.91 at the highest turbulence intensity cases. The Strouhal number exerts a similar influence, as it multiplies $\sigma_{T,D}$, and is therefore responsible for the drop in magnitude of the local maxima with increasing frequency. For example, the highest turbulence intensity case gain has values of 0.91, 0.87, and 0.83 for the first three local maxima.

There are also competing effects in area and burning rate terms. Consider Eq. (41): the magnitude of the third term, representing fluctuations due to burning rate increases with increasing turbulent Markstein lengths, while the first term, representing area changes decreases. That is, increasing the turbulent displacement Markstein length increases the rate of wrinkle destruction, which reduces the integration limit corrections and therefore the area fluctuations arising from those corrections.

This point can be seen from Fig. 9 , which shows the magnitude of the individual contributions to the *FTF*, where the contribution from the downstream integration limit correction is denoted G_W, and the upstream integration limit correction is denoted G_I; collectively these two

‡ Note, however, that the numerical results and non-linear analytical integration (see Fig. 7) show that the *FDF* gain can increase with turbulence if the mean flame speed and flame slope changes with downstream distance.

contributions are equal to G_A. Note that the magnitude of G_I stays constant, while the magnitude of G_W decreases with increasing Strouhal number. This reflects the fact that at higher St_{Lf} there is more time / distance for flame wrinkles to decay downstream and consequently the area fluctuation and contribution to the *FTF* are reduced. Additionally, Fig. 9 shows the contribution due to the non-constant consumption speed, G_S, given in Eq. (37). Clearly, area fluctuations dominate the *FTF*, rather than the consumption speed correction. Ultimately, the small contribution due to the consumption speed correction reflects the fact that the consumption speed differs little from $s_{T,0}$ for this linear analysis. This is not to say, however, that the effect of $\sigma_{T,D}$ is insignificant. On the contrary, $\sigma_{T,D}$ has a large effect on the *FTF*, but that effect occurs through changes to the flame *area*, rather than the flame *speed*. The right side of Fig. 8 shows the phase of the analytical *FTFs.* For increasing values of $\sigma_{T,D}$, the phase change across the gain minima becomes smoother.

Comparing the analytical results in Fig. 8 to the numerical simulation results presented in Fig. 7, it is clear that this model problem correctly predicts the general qualitative shape of the numerical *FDF* – specifically, the progressive decrease of *FTF* gain maxima, and increase of gain minima, with increasing Strouhal number.

The qualitative features of the phase are also predicted by the model. The phase increases linearly with increasing Strouhal number, jumping across the gain minima. In addition, the stochastic fluctuations smooth the gain jumps, similar to the numerical simulation. Finally, it is clear that the linear, analytical model displays higher gain maxima values. This difference results from nonlinear effects which spread the heat release response spectral energy over higher harmonics of the forcing frequency, and in turn decrease the amplitude of the *FDF* at the forcing frequency.

B. Model Problem: Flame Perturbed by Convecting, Decaying Vortex

As described earlier, the oscillating flame holder problem is an important one from a pedagogical perspective. In this section, we consider a problem that has additional complexities, but is of significant interest as a practical problem. Specifically, this section considers the response of a flame to a convecting disturbance, generalizing the laminar *FTF* work previously presented in several studies (Schuller et al., 2003, Preetham et al., 2008, Preetham et al., 2010). While a fully general treatment of this problem requires numerical treatment as in Sec. IV, we consider here a V-flame model problem which is quite similar to several of the prior laminar studies. We retain the same assumptions as in Sec. V.A, except here the flame holder is fixed and there is a harmonically oscillating flow disturbance, whose component normal to the nominal flame position is given by:

$$u_{n,1} = \text{Real}\left\{ \varepsilon \cdot u_{s,eff} \cdot e^{-\gamma \frac{\omega_d \cdot s}{2\pi u_{s,eff}}} \cdot e^{i\frac{\omega_d \cdot s}{u_C}} \cdot e^{-i\omega_d t} \right\} \tag{43}$$

where ε is a non-dimensional velocity perturbation amplitude, γ is a non-dimensional decay rate, and u_c is the velocity disturbance phase speed along the flame coordinate. The derivation of the flame position and *FTF* are given in the appendix. The resulting Fourier space fluctuating flame position is:

$$\left\langle \hat{\xi}'\left(\omega_d, s\right)\right\rangle = \frac{e^{sR_1} - e^{s\frac{\omega_d}{u_{s,eff}}P}}{\frac{S_{T,0}\sigma_{T,D}}{u_{s,eff}}\left(\frac{\omega_d}{u_{s,eff}}\right)^2 P^2 - \frac{\omega_d}{u_{s,eff}}P + i\frac{\omega_d}{u_{s,eff}}}, \qquad P = \left(i\frac{u_{s,eff}}{u_C} - \frac{\gamma}{2\pi} \right) \tag{44}$$

This solution can be expanded around small σ values as:

$$\left\langle \hat{\xi}'\left(\omega_d, s\right)\right\rangle = \frac{\exp\left[s\left(\frac{i\omega_0}{u_{s,eff}} - \frac{\omega_0^2 S_{T,0}\sigma_{T,D}}{u_{s,eff}^{\ 3}}\right)\right] - \exp\left[s\frac{\omega_d}{u_{s,eff}}\left(i\frac{u_{s,eff}}{u_C} - \frac{\gamma}{2\pi}\right)\right]}{\frac{\omega_d}{u_{s,eff}}\left(i-P\right)}\left(1-\sigma_{T,D}\frac{S_{T,0}\omega_d P^2}{u_{s,eff}^{\ 2}\left(i-P\right)}\right) \quad (45)$$

Non-dimensionalizing the *FTF*, according to the scheme given in Eq. (40), gives:

$$\hat{G}_{Tot}\left(\omega_d\right) = \frac{e^{St_{L_f}\tilde{P}} - e^{St_{L_f}\tilde{R}_1} + \tan\left(\theta\right)\tilde{\sigma}_{T,C}\left[\tilde{R}_1\left(e^{St_{L_f}\tilde{R}_1} - 1\right) + \tilde{P}\left(1 - e^{St_{L_f}\tilde{P}}\right)\right]}{St_{L_f}\left(\tilde{S}_{T,0}\tilde{\sigma}_{T,D}\tilde{P}^2 - \tilde{P} + i\right)} \quad (46)$$

Additionally, Eq. (46) can be expanded for small turbulent Markstein lengths as:

$$\hat{G}_{Tot}\left(\omega_d\right) = \frac{\left(e^{St_{L_f}\tilde{P}} - e^{St_{L_f}\left(i-\tilde{S}_{T,0}\tilde{\sigma}_{T,D}\right)}\right)\left(1 - \frac{\tilde{S}_{T,0}\tilde{P}^2}{\left(i-\tilde{P}\right)}\tilde{\sigma}_{T,D}\right) + \tan\left(\theta\right)\tilde{\sigma}_{T,C}\left[i\left(e^{St_{L_f}\left(i-\tilde{S}_{T,0}\tilde{\sigma}_{T,D}\right)} - 1\right) + \tilde{P}\left(1 - e^{St_{L_f}\tilde{P}}\right)\right]}{St_{Lf}\left(i-\tilde{P}\right)} \quad (47)$$

Figure 10 shows the *FTF* gain and phase for the convecting, decaying velocity disturbance perturbed V-flame. For comparison to the oscillating flame holder model problem, the same values of $S_{T,0}$, $\sigma_{T,D}$, and $\sigma_{T,C}$ are used. The gain of the *FTF* shows the characteristic magnitude roll-off with increasing Strouhal number. In the bulk forcing case (i.e., $u_{s,eff}/u_c = 0$), with no disturbance velocity decay $(\gamma = 0)$, the turbulent, ensemble-averaged *FTF* reverts to the same as that previously derived for a stretch-sensitive, bulk-forced laminar flame (Wang et al., 2009, Preetham et al., 2010).

The effect of increasing turbulence, with a resultant increase in the turbulent Markstein length, is less pronounced for the convecting, decaying velocity disturbance than for the oscillating flame holder model problem, but still results in a similar effect; increasing turbulence decreases the *FTF* gain maxima. The phase plot of the *FTF* shown in Fig. 10 shows the influence of the convecting velocity disturbance. Note the near linear dependence of the phase with

Strouhal number for low Strouhal values, implying that the flame can be described by a lumped, fixed time delay model in this region.

The close correspondence between the *FTFs* at different turbulence intensities indicates why the quasi-laminar approach has been successful for prediction of turbulent flame response to harmonic disturbances. The *FTF* of the convecting, decaying vortex problem is not strongly dependent on turbulence intensity.

VI. Conclusions

This paper examines the global heat release response of turbulent, premixed, flames subjected to harmonic forcing of the flame holder. The position of the ensemble-averaged flame is determined by application of a definition for the effective turbulent flame speed, given by Shin and Lieuwen (2013). The curvature sensitivity of the ensemble-averaged flame is accounted for by inclusion of a curvature dependent flame speed, which is a function of the turbulent Markstein length. Validation for the closure model is provided by comparison to a numerically simulated flame. For low to moderate turbulence intensities, the model predicts a nearly identical flame shape and closely approximates the gain and phase of *FDF*. Furthermore, these results demonstrate that a key qualitative trend predicted by the burning velocity closure – the progressive decrease in maxima and increase in minima with Strouhal number – is also observed in the ensemble-averaged computational results.

Together, these results show that it is possible to model the response of a turbulent flame perturbed by both narrowband harmonic oscillations and broadband turbulence though analysis of the ensemble-averaged flame, for low to moderate stochastic amplitudes. Furthermore, this approach is able to capture some of the nonlinear effects of turbulence (i.e. kinematic restoration) even in a linearized model. This approach is analogous to that used with laminar flames, and uses

a modified flame position equation, as well as an ensemble-averaged flame speed closure with a Markstein like dependence on the ensemble-averaged flame curvature.

Two linear model problems are also presented. The first derives the *FTF* for the oscillating flame holder problem. These linear models show that it is possible to capture several of the key effects of stochastic disturbances on the *FTF*. Specifically, the linear model predicts increasing Strouhal number simultaneously decreases gain maxima and increases gain minima. *FTF* phase trends also qualitatively match the numerical results. The second model problem investigates a flame attached to a stationary flame holder, but perturbed by a convecting decaying velocity fluctuation. Similar to the first model problem, increasing turbulence decreases the gain maxima.

Appendix: Derivation of Convecting Vortex Model Problem

Application of the given assumptions to Eq. (21) leads to the following ordinary partial differential equation for the Fourier transformed flame position:

$$\frac{\partial^2 \left\langle \hat{\xi}'(s) \right\rangle}{\partial s^2} - \frac{\partial \left\langle \hat{\xi}'(s) \right\rangle}{\partial s} \frac{\left\langle u_{s,eff} \right\rangle}{S_{T,0}\sigma_{T,D}} + \left\langle \hat{\xi}'(s) \right\rangle \frac{i\omega_d}{S_{T,0}\sigma_{T,D}} + \frac{u_{s,eff}}{S_{T,0}\sigma_{T,D}} \exp\left[s \frac{\omega_d}{u_{s,eff}} \left(i \frac{u_{s,eff}}{u_C} - \frac{\gamma}{2\pi} \right) \right] = 0 \quad \text{(A1)}$$

This equation has the same homogeneous solution as Eq. (25), but a different particular solution due to the nature of the harmonic forcing. The solution of the Fourier space flame fluctuation is given by:

$$\hat{\xi}'(\omega_d, s) = Ae^{sR_1} + Be^{sR_2} - \frac{u_{s,eff} \exp\left[s \frac{\omega_d}{u_{s,eff}} \left(i \frac{u_{s,eff}}{u_C} - \frac{\gamma}{2\pi} \right) \right]}{S_{T,0}\sigma_{T,D} \left(\frac{\omega_d}{u_{s,eff}} \right)^2 \left(i \frac{u_{s,eff}}{u_C} - \frac{\gamma}{2\pi} \right)^2 - \omega_d \left(i \frac{u_{s,eff}}{u_C} - \frac{\gamma}{2\pi} \right) + i\omega_d} \quad \text{(A2)}$$

where $R_{1,2}$ are defined according to Eq. (29). This equation is solved subject to the stationary flame-attachment boundary condition:

$$\xi_1(s=0,t)=0 \tag{A3}$$

As with the oscillating flame holder model problem, the second boundary condition stipulates that no information propagates upstream. Therefore the *B* coefficient is set to zero. The resulting Fourier space fluctuating flame position is:

$$\left\langle \hat{\xi}'(\omega_d,s)\right\rangle = \frac{e^{sR_1}-e^{s\frac{\omega_d}{u_{s,eff}}P}}{\frac{S_{T,0}\sigma_{T,D}}{u_{s,eff}}\left(\frac{\omega_d}{u_{s,eff}}\right)^2 P^2-\frac{\omega_d}{u_{s,eff}}P+i\frac{\omega_d}{u_{s,eff}}}, \qquad P=\left(i\frac{u_{s,eff}}{u_C}-\frac{\gamma}{2\pi}\right) \tag{A4}$$

This solution can be expanded around small σ values as:

$$\left\langle \hat{\xi}'(\omega_d,s)\right\rangle = \frac{\exp\left[s\left(\frac{i\omega_0}{u_{s,eff}}-\frac{\omega_0^2 S_{T,0}\sigma_{T,D}}{u_{s,eff}^{\ 3}}\right)\right]-\exp\left[s\frac{\omega_d}{u_{s,eff}}\left(i\frac{u_{s,eff}}{u_C}-\frac{\gamma}{2\pi}\right)\right]}{\frac{\omega_d}{u_{s,eff}}(i-P)}\left[1-\sigma_{T,D}\frac{S_{T,0}\omega_d P^2}{u_{s,eff}^{\ 2}(i-P)}\right] \tag{A5}$$

Unlike the oscillating flame holder problem, with the velocity forced case only a downstream integration limit correction is required, because the flame attachment point is stationary. This end correction, determined in the same manner as described in Sec. V.A is:

$$\Delta\hat{s}_{W,1}=\frac{-\varepsilon}{\tan(\theta)}\frac{e^{s_W R_1}-e^{s_W\frac{\omega_d}{u_{s,eff}}P}}{\frac{S_{T,0}\sigma_{T,D}}{u_{s,eff}}\left(\frac{\omega_d}{u_{s,eff}}\right)^2 P^2-\frac{\omega_d}{u_{s,eff}}P+i\frac{\omega_d}{u_{s,eff}}} \tag{A6}$$

The general form of the heat release, after linearization, is given below.

$$Q(t)=\int_0^{s_{W,1}(t)}\rho\Delta h_r S_{T,C0}(s)\left(1+\sigma_{T,C}(s)\frac{\partial^2\xi_1}{\partial s^2}\right)ds \tag{A7}$$

Assuming spatially constant $S_{T,C0}$ and $\sigma_{T,C}$, integration of Eq. (A7) yields:

$$\hat{Q}(\omega_d) = \rho \Delta h_r S_{T,C0} \varepsilon \left\{ \frac{\sigma_{T,C}\left[R_1\left(e^{L_f R_1} - 1\right) + P\frac{\omega_d}{u_{s,eff}}\left(1 - e^{L_f \frac{\omega_d}{u_{s,eff}} P}\right)\right] - \frac{1}{\tan(\theta)}\left(e^{L_f R_1} - e^{L_f \frac{\omega_d}{u_{s,eff}} P}\right)}{\frac{S_{T,0}\sigma_{T,D}}{u_{s,eff}}\left(\frac{\omega_d}{u_{s,eff}}\right)^2 P^2 - \frac{\omega_d}{u_{s,eff}} P + i\frac{\omega_d}{u_{s,eff}}} \right\} \quad \text{(A8)}$$

The normal component of the coherent velocity fluctuation at the flame anchor provides the reference flow disturbance.

$$u'_{n,ref} = \hat{u}_{n,1}(s=0) = \varepsilon \cdot u_{s,eff} \quad \text{(A9)}$$

This velocity disturbance, after normalization by $u_{n,0}$, becomes:

$$\frac{\hat{u}'_{n,ref}}{u_{n,0}} = \frac{\varepsilon}{\tan(\theta)} \quad \text{(A10)}$$

Then, the resulting *FTF* according to Eq. (5) is

$$\hat{G}_{Tot}(\omega_d) = \frac{e^{L_f \frac{\omega_d}{u_{s,eff}} P} - e^{L_f R_1} + \tan(\theta)\sigma_{T,C}\left[R_1\left(e^{L_f R_1} - 1\right) + \frac{\omega_d}{u_{s,eff}} P\left(1 - e^{L_f \frac{\omega_d}{u_{s,eff}} P}\right)\right]}{St_{L_f}\left(\frac{S_{T,0}\sigma_{T,D}}{u_{s,eff}}\left(\frac{\omega_d}{u_{s,eff}}\right) P^2 - P + i\right)} \quad \text{(A11)}$$

This expression can be non-dimensionalized according to the scheme given in Eq. (40) as:

$$\hat{G}_{Tot}(\omega_d) = \frac{e^{St_{L_f}\tilde{P}} - e^{St_{L_f}\tilde{R}_1} + \tan(\theta)\tilde{\sigma}_{T,C}\left[\tilde{R}_1\left(e^{St_{L_f}\tilde{R}_1} - 1\right) + \tilde{P}\left(1 - e^{St_{L_f}\tilde{P}}\right)\right]}{St_{L_f}\left(\tilde{S}_{T,0}\tilde{\sigma}_{T,D}\tilde{P}^2 - \tilde{P} + i\right)} \quad \text{(A12)}$$

Eq. (46) can be expanded for small turbulent Markstein lengths as:

$$\hat{G}_{Tot}(\omega_d) = \frac{\left(e^{St_{L_f}\tilde{P}} - e^{St_{L_f}\left(i - \tilde{S}_{T,0}\tilde{\sigma}_{T,D}\right)}\right)\left(1 - \frac{\tilde{S}_{T,0}\tilde{P}^2}{\left(i - \tilde{P}\right)}\tilde{\sigma}_{T,D}\right) + \tan(\theta)\tilde{\sigma}_{T,C}\left[i\left(e^{St_{L_f}\left(i - \tilde{S}_{T,0}\tilde{\sigma}_{T,D}\right)} - 1\right) + \tilde{P}\left(1 - e^{St_{L_f}\tilde{P}}\right)\right]}{St_{L_f}\left(i - \tilde{P}\right)} \quad \text{(A13)}$$

Acknowledgements

This work has been partially sponsored by the NASA Aeronautics Scholarship Program through grant number NNX14AE98H, and the National Science Foundation contract CBET-1235779 (contract monitor Professor Ruey-Hung Chen).

References

1. Acharya, V., Emerson, B., Mondragon, U., Shin, D.-H., Brown, C., Mcdonell, V., and Lieuwen, T. 2013. Velocity and flame wrinkling characteristics of a transversely forced, bluff-body stabilized flame, part ii: Flame response modeling and comparison with measurements. *Combust. Sci. Technol.,* 185**,** 1077-1097.
2. Acharya, V., Malanoski, M., Aguilar, M., and Lieuwen, T. 2014. Dynamics of a transversely excited swirling, lifted flame: Flame response modeling and comparison with experiments. *Journal of Engineering for Gas Turbines and Power,* 136**,** 051503(1)-051503(10).
3. Barkley, D. 2006. Linear analysis of the cylinder wake mean flow. *Europhys. Lett.,* 75**,** 750-756.
4. Boyer, L., and Quinard, J. 1990. On the dynamics of anchored flames. *Combust. Flame,* 82**,** 51-65.
5. Candel, S. 2002. Combustion dynamics and control: Progress and challenges. *Proc. Combust. Inst.,* 29**,** 1-28.
6. Creta, F., Fogla, N., and Matalon, M. 2011. Turbulent propagation of premixed flames in the presence of darrieus-landau instability. *Combustion Theory and Modelling,* 15**,** 267-298.

7. Cuquel, A., Durox, D., and Schuller, T. 2013. Impact of flame base dynamics on the non-linear frequency response of conical flames. *Comptes Rendus Mécanique,* 341**,** 171-180.
8. Ducruix, S., Durox, D., and Candel, S. 2000. Theoretical and experimental determination of the transfer function of a laminar premixed flame. *Proc. Combust. Inst.,* 28**,** 765-773.
9. Ducruix, S., Schuller, T., Durox, D., and Candel, S. 2003. Combustion dynamics and instabilities: Elementary coupling and driving mechanisms. *J. Propul. Power,* 19**,** 722-734.
10. Dupont, T. F., and Liu, Y. 2007. Back and forth error compensation and correction methods for semi-lagrangian schemes with application to level set interface computations. *Mathematics of Computation,* 76**,** 647-668.
11. Fleifil, M., Annaswamy, A. M., Ghoneim, Z. A., and Ghoneim, A. F. 1996. Response of a laminar premixed flame to flow oscillations: A kinematic model and thermoacoustic instability results. *Combust. Flame,* 106**,** 487-510.
12. Hemchandra, S., Peters, N., and Lieuwen, T. 2011. Heat release response of acoustically forced turbulent premixed flames—role of kinematic restoration. *Proc. Combust. Inst.,* 33**,** 1609-1617.
13. Hemchandra, S., Preetham, and Lieuwen, T. C. 2007. Response of turbulent premixed flames to harmonic acoustic forcing. *Proc. Combust. Inst.,* 31**,** 1427-1434.
14. Hinze, J. 1975. *Turbulence,* New York, McGraw-Hill.
15. Humphrey, L., Acharya, V., Shin, D. H., and Lieuwen, T. 2014. Technical note: Coordinate systems and integration limits for global flame transfer function calculations. *Int. J. Spray and Combust. Dyn.,* 6**,** 411-416.
16. Jiang, G.-S., and Peng, D. 2000. Weighted eno schemes for hamilton-jacobi equations. *SIAM Journal on Scientific Computing,* 21**,** 2126-2143.

17. Jones, B., Lee, J. G., Quay, B. D., and Santavicca, D. A. 2011. Flame response mechanisms due to velocity perturbations in a lean premixed gas turbine combustor. *Journal of Engineering for Gas Turbines and Power,* 133**,** 021503-021503.
18. Kanthasamy, C., Raghavan, V., and Srinivasan, K. 2012. Effect of low frequency burner vibrations on the characteristics of premixed flames. *Int. J. Spray and Combust. Dyn.,* 4**,** 239-254.
19. Kashinath, K., Hemchandra, S., and Juniper, M. P. 2013. Nonlinear thermoacoustics of ducted premixed flames: The influence of perturbation convection speed. *Combust. Flame,* 160**,** 2856-2865.
20. Kerstein, A. R., Ashurst, W. T., and Williams, F. A. 1988. Field equation for interface propagation in an unsteady homogeneous flow field. *Physical Review A,* 37**,** 2728.
21. Kornilov, V. N., Schreel, K. R. a. M., and De Goey, L. P. H. 2007. Experimental assessment of the acoustic response of laminar premixed bunsen flames. *Proc. Combust. Inst.,* 31**,** 1239-1246.
22. Lee, D. H., and Lieuwen, T. C. 2003. Premixed flame kinematics in a longitudinal acoustic field. *Journal of Propulsion and Power,* 19**,** 837-846.
23. Lieuwen, T. C., and Yang, V. (eds.) 2005. *Combustion instabilities in gas turbine engines: Operational experience, fundamental mechanisms, and modeling*: American Institute of Aeronautics and Astronautics.
24. Lipatnikov, A. N., and Sathiah, P. 2005. Effects of turbulent flame development on thermoacoustic oscillations. *Combust. Flame,* 142**,** 130-139.
25. Matalon, M., and Matkowsky, B. J. 1982. Flames as gasdynamic discontinuities. *Journal of Fluid Mechanics Digital Archive,* 124**,** 239-259.

26. Meliga, P., Pujals, G., and Serre, É. 2012. Sensitivity of 2-d turbulent flow past a d-shaped cylinder using global stability. *Phys. Fluids,* 24.

27. Mettot, C., Sipp, D., and Bézard, H. 2014. Quasi-laminar stability and sensitivity analyses for turbulent flows: Prediction of low-frequency unsteadiness and passive control. *Phys. Fluids,* 26.

28. Peters, N., Wenzel, H., and Williams, F. A. 2000. Modification of the turbulent burning velocity by gas expansion. *Proc. Combust. Inst.,* 28**,** 235-243.

29. Petersen, R. E., and Emmons, H. W. 1961. Stability of laminar flames. *Phys. Fluids (1958-1988),* 4**,** 456-464.

30. Pope, S. 2000. *Turbulent flows,* New York, Cambridge Univ Press.

31. Preetham, Santosh, H., and Lieuwen, T. 2008. Dynamics of laminar premixed flames forced by harmonic velocity disturbances. *J. Propul. Power,* 24**,** 1390-1402.

32. Preetham, T., Thumuluru, S. K., Santosh, H., and Lieuwen, T. 2010. Linear response of laminar premixed flames to flow oscillations: Unsteady stretch effects. *J. Propul. Power,* 26**,** 524-532.

33. Schuller, T., Ducruix, S., Durox, D., and Candel, S. 2002. Modeling tools for the prediction of premixed flame transfer functions. *Proc. Combust. Inst.,* 29**,** 107-113.

34. Schuller, T., Durox, D., and Candel, S. 2003. A unified model for the prediction of laminar flame transfer functions: Comparisons between conical and v-flame dynamics. *Combust. Flame,* 134**,** 21-34.

35. Shanbhogue, S., Shin, D.-H., Hemchandra, S., Plaks, D., and Lieuwen, T. 2009. Flame-sheet dynamics of bluff-body stabilized flames during longitudinal acoustic forcing. *Proc. Combust. Inst.,* 32**,** 1787-1794.

36. Shin, D.-H., and Lieuwen, T. 2012. Flame wrinkle destruction processes in harmonically forced, laminar premixed flames. *Combust. Flame,* 159**,** 3312-3322.

37. Shin, D. H., and Lieuwen, T. C. 2013. Flame wrinkle destruction processes in harmonically forced, turbulent premixed flames. *J. Fluid Mech.,* 721**,** 484-513.

38. Shin, D. H., Lieuwen, T. C., and Shanbhogue, S. 2008. Premixed flame kinematics in an axially decaying, harmonically oscillating vorticity field. *44th AIAA/ASME/SAE/ASEE Joint Propulsion Conference & Exhibit.* American Institute of Aeronautics and Astronautics.

39. Wang, H. Y., Law, C. K., and Lieuwen, T. 2009. Linear response of stretch-affected premixed flames to flow oscillations. *Combust. Flame,* 156**,** 889-895.

40. Williams, F. A. 1985. Turbulent combustion. *In:* BUCKMASTER, J. D. (ed.) *The mathematics of combustion.* Philadelphia: Society for Industrial and Applied Mathematics.

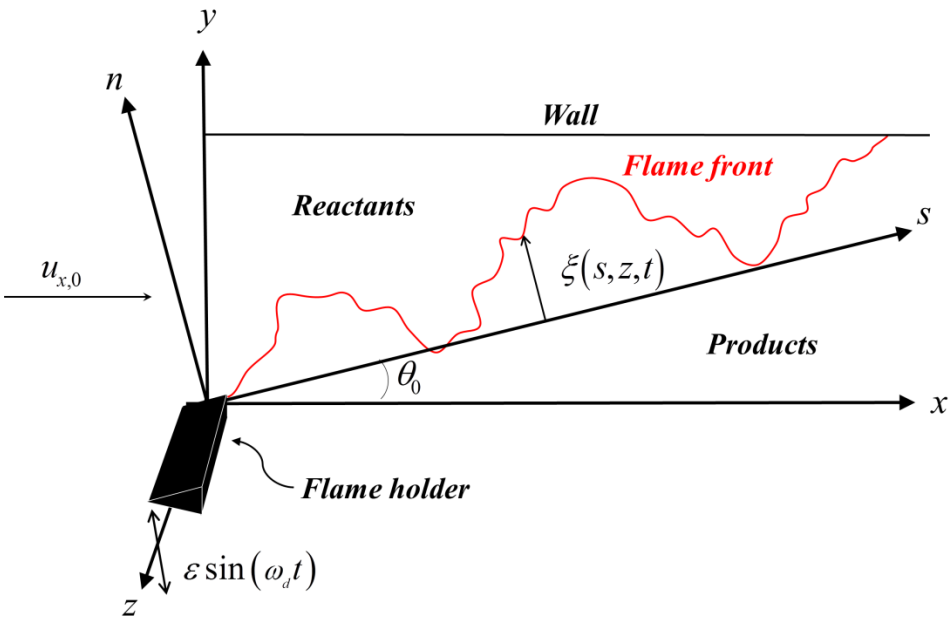

Figure 1. Schematic of flame geometry and coordinate systems.

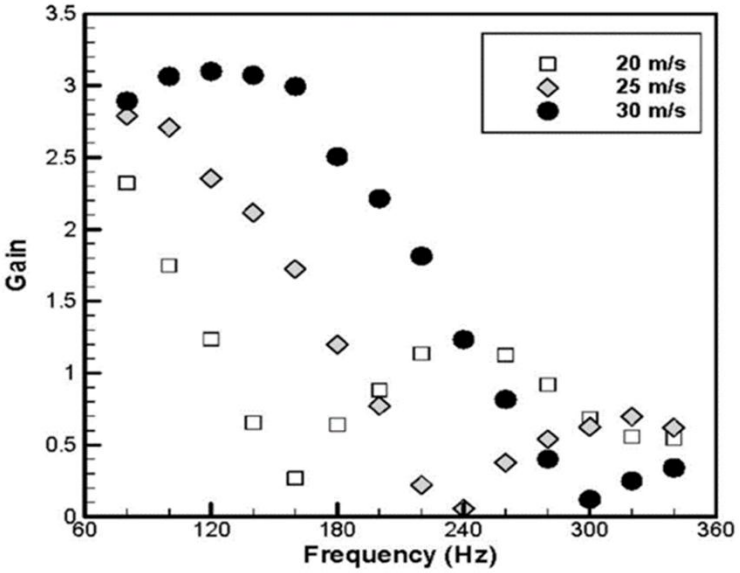

Figure 2. Experimentally determined *FDF* gain for a turbulent premixed, swirl-stabilized flame at three mean flow velocities, from (Jones et al., 2011).

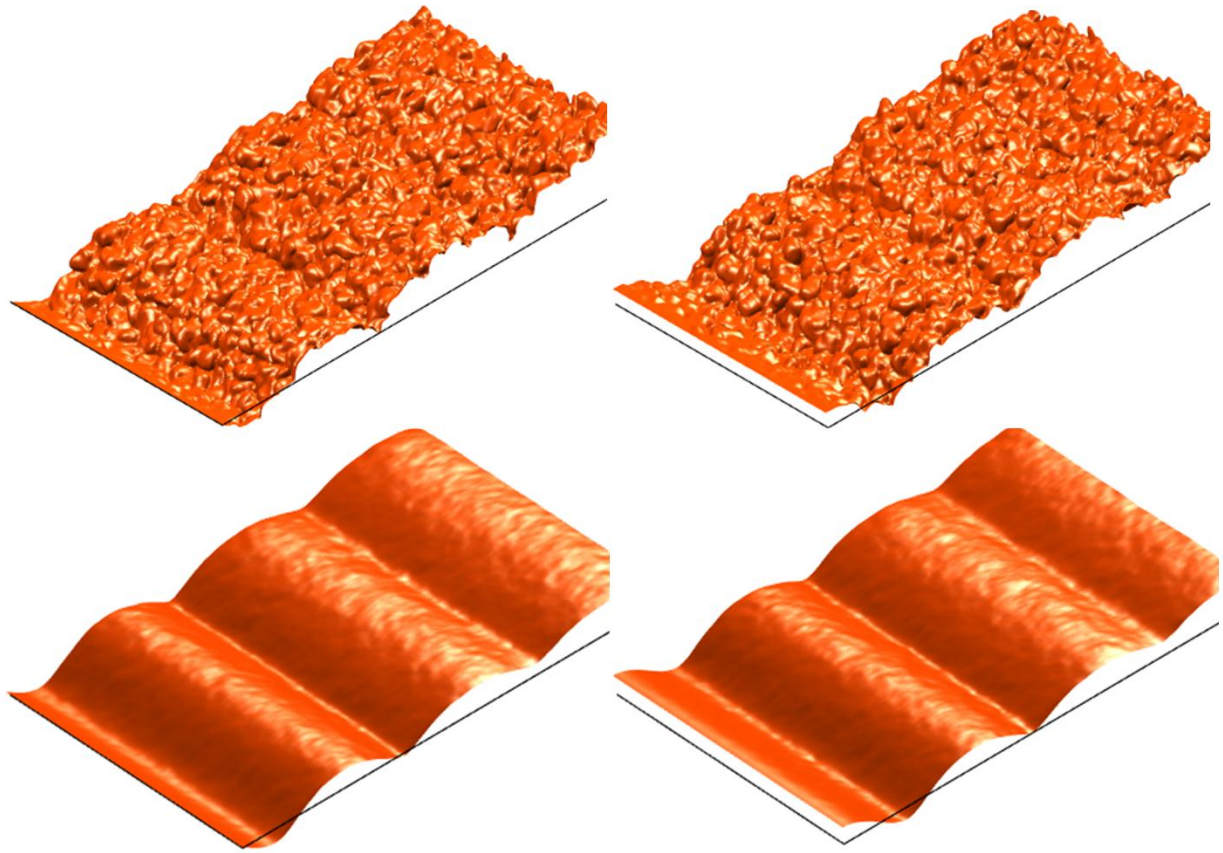

Figure 3. Snapshots of the instantaneous flame surface (top) and ensemble-averaged result (bottom) at two time instances, $t\cdot\omega_d = 0$ (left) and $t\cdot\omega_d = \pi/2$ (right). Data shown for a turbulent field with $L_{11}/\varepsilon = 0.5$, $\varepsilon/(u_{S,0}/\omega_d) = 0.65$, $u_{RMS}/u_{s,0} = 0.082$.

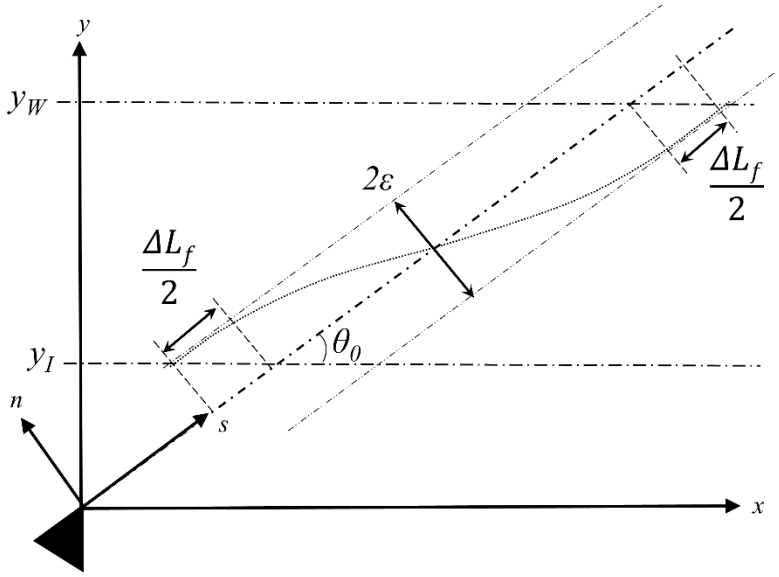

Figure 4. Illustration of flame length fluctuation.

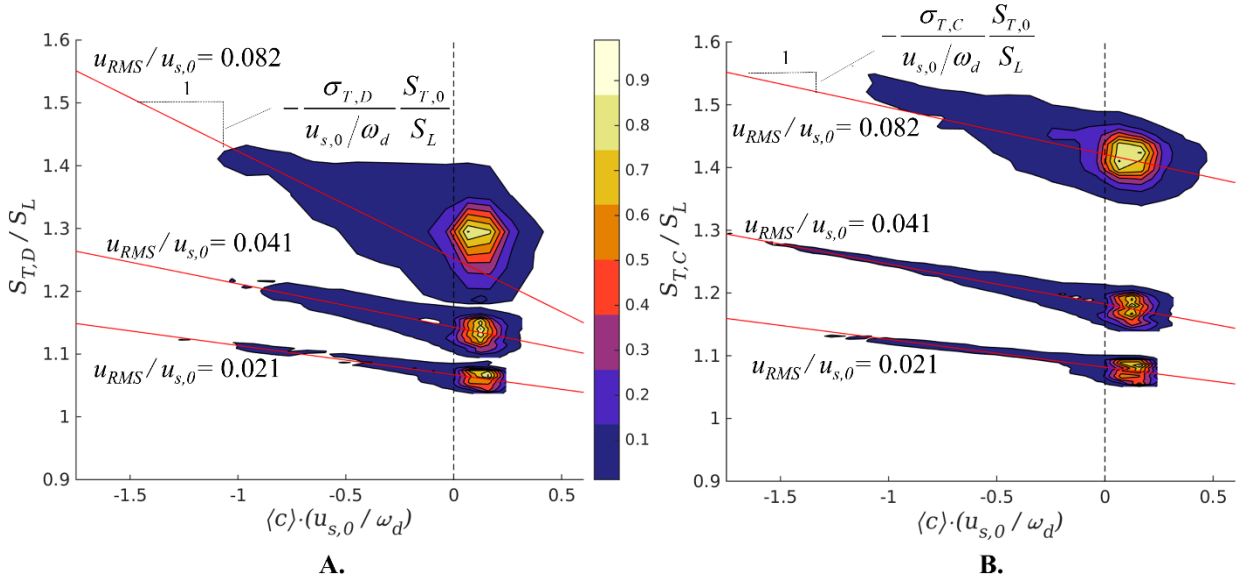

Figure 5. Joint probability density function plots showing the normalized, non-dimensional A) effective turbulent displacement speed and B) effective turbulent consumption speed versus ensemble-averaged flame curvature. The turbulent Markstein lengths are derived from the slope of the linear regressions. Data shown for a turbulent field with L_{11}/ε = 0.5, $\varepsilon/(u_{s,0}/\omega_d)$ = 0.65.

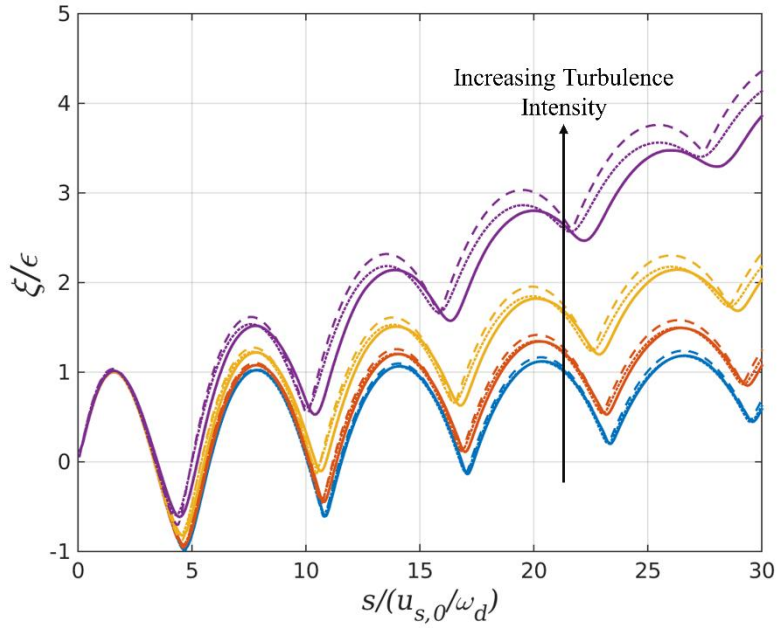

Figure 6. Ensemble-averaged flame position calculated from numerical solution of the *G*-equation (solid lines), integration of Eq. (24) (dotted lines), and "quasi-laminar" result (dashed lines). Data shown for a turbulent field with L_{11}/ε = 0.5, $\varepsilon/(u_{S,0}/\omega_d)$ = 0.65, $t\cdot\omega_d = \pi$, and $u_{RMS}/u_{s,0}$ = 0.010, 0.021, 0.041, 0.082.

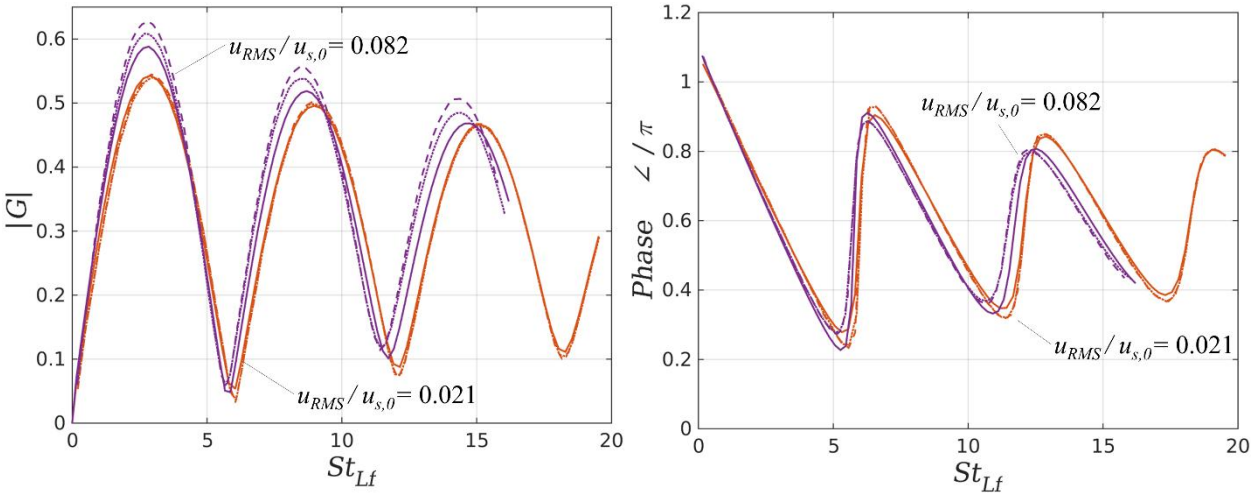

Figure 7. Flame describing function gain (left) and phase (right) calculated from the numerical solution of the *G*-equation (solid lines), integration of Eq. (23) (dotted lines), and quasi-laminar result (dashed lines). Data shown for a turbulent field with L_{11}/ε = 0.5, $\varepsilon/(u_{S,0}/\omega_d)$ = 0.65, at two turbulence intensities.

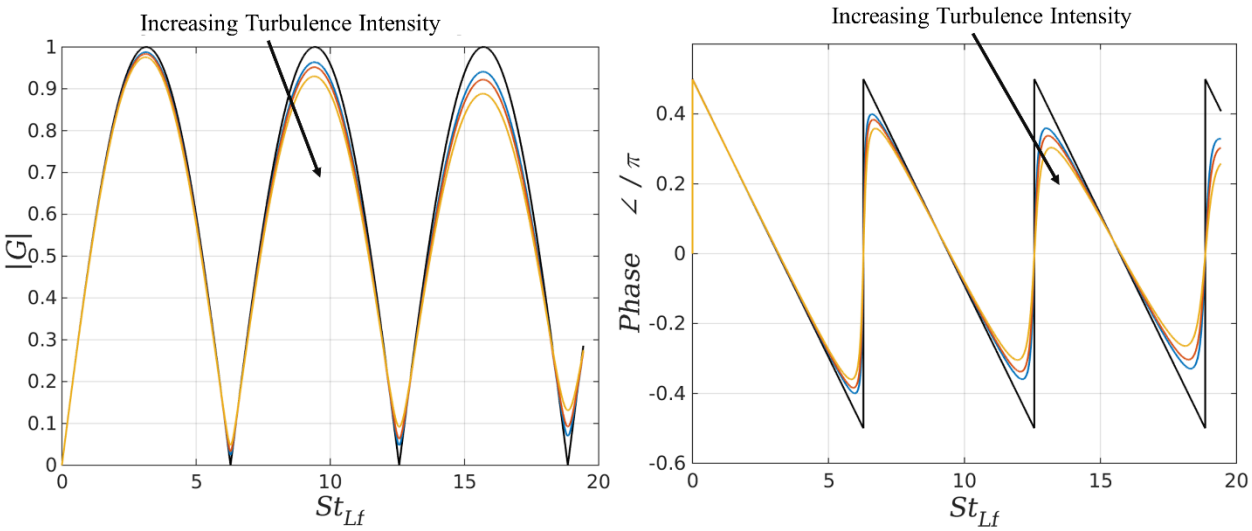

Figure 8. Analytical *FTF* gain (left), and phase (right) as a function of St_{Lf}, for a turbulent field with L_{11}/ε = 0.5, $\varepsilon/(u_{S,0}/\omega_d)$ = 0.65, $\sigma_{T,D}/(u_{S,0}/\omega_d)$ = 0.0, 0.0313, 0.0408, and 0.0568, for the turbulence intensities from $u_{RMS}/u_{S,0}$= 0 to 0.041, respectively.

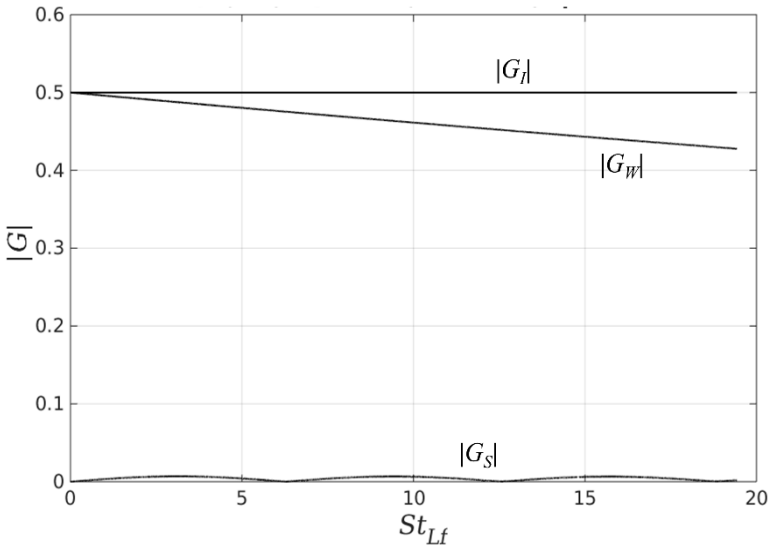

Figure 9. Individual contributions to the analytical *FTF*, for a turbulent field with $L_{11}/\varepsilon = 0.5$, $\varepsilon/(u_{S,0}/\omega_d) = 0.65$, $u_{RMS}/u_{S,0} = 0.01$. G_I, G_W, and G_S are the contributions due to the start correction, wall correction, and consumption speed, respectively.

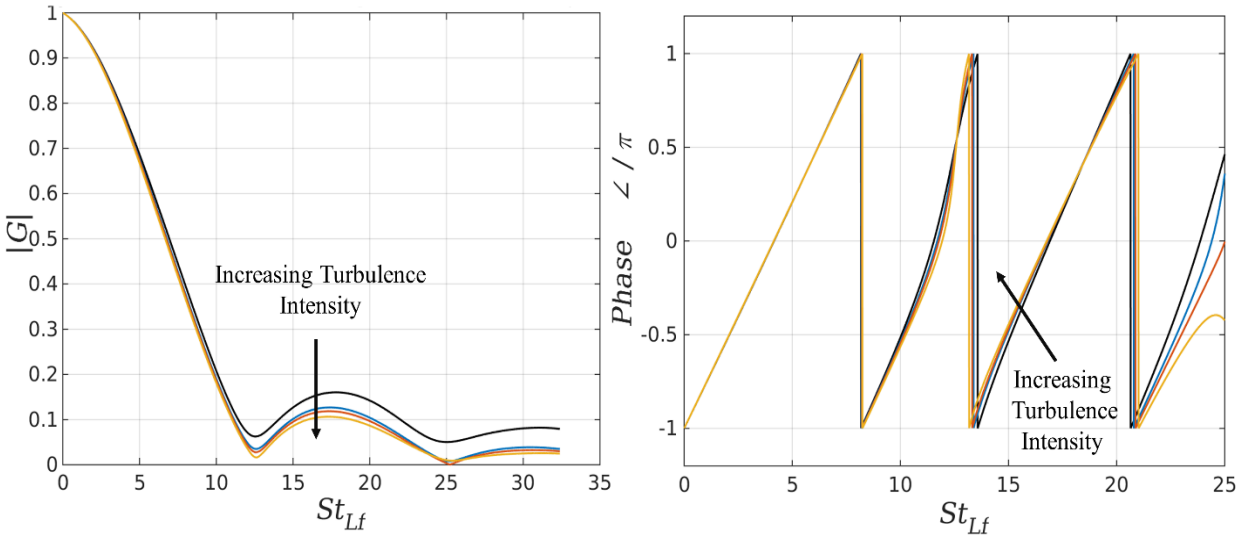

Figure 10. Analytical *FTF* gain (left), and phase (right) for a V-flame perturbed by a convecting, decaying velocity perturbation, $u_{S,0}/u_c$ = 0.5, γ = 0.25, as a function of St_{Lf}, for a turbulent field with L_{11}/ε = 0.5, $\varepsilon/(u_{S,0}/\omega_d)$ = 0.65, $\sigma_{T,D}/(u_{S,0}/\omega_d)$ = 0.0, 0.0313, 0.0408, and 0.0568, for the turbulence intensities from $u_{RMS}/u_{S,0}$ = 0 to 0.041, respectively.